APPLIED PHYSICS LETTERS **104**, 183501 (2014)

Bipolar and unipolar resistive switching modes in Pt/$Zn_{0.99}Zr_{0.01}O$/Pt structure for multi-bit resistance random access memory

D. L. Xu,[1] Y. Xiong,[2] M. H. Tang,[1,a)] B. W. Zeng,[1] and Y. G. Xiao[1]
[1]*Key Laboratory of Low Dimensional Materials and Application Technology of Ministry of Education, Xiangtan University, Xiangtan, Hunan 411105, China*
[2]*The School of Mathematics and Computational Science, Xiangtan University, Xiangtan, Hunan 411105, People's Republic of China*

(Received 23 October 2013; accepted 27 April 2014; published online 5 May 2014)

In this work, we report the coexistence of bipolar resistive switching (BRS) and unipolar resistive switching (URS) modes in Pt/$Zn_{0.99}Zr_{0.01}O$/Pt structure device. After the forming process, this device with URS behavior exhibits either URS mode in the same direction or BRS mode in the opposite direction during the reset process. Controllable multi-state resistances in the low and high resistance states for the BRS mode were obtained by imposing different compliance currents (I_{cc}) and the span of voltage sweeping in the reset process (V_{stop}). These results suggest that our devices have high potential for the next generation of nonvolatile memory applications. © *2014 AIP Publishing LLC*. [http://dx.doi.org/10.1063/1.4875383]

As the potential next generation for nonvolatile memory, the transition metal oxide (TMO)-based resistance random access memories (RRAMs) have been studied intensively during the past decade and have attracted increasing interest, mainly due to their low power consumption, high operation speed, high endurance, and simplicity in structure.[1–3] Based on the dependence of switching characteristic on electric polarity, there are two different types of resistive switching (RS) modes: unipolar RS (URS) mode and bipolar RS (BRS) mode.[4] Generally, either URS or BRS has been reported for a single system with different characteristics observations. For example, URS exhibits higher resistance ratio (high resistance state (HRS) to low resistance state (LRS) (R_{HRS}/R_{LRS})), easier reading operation, and higher memory density.[5] While BRS features faster switching speed, lower operation power, and better endurance.[6] It would be advantageous to develop scalable material devices possessing both the BRS and URS modes in order to expand the devices application scope of non-volatile memories.

In recent reports, the ZnO-based thin films were reported to simultaneously exhibit the BRS and URS modes with the usage of different electrode materials,[7,8] by controlling compliance currents (I_{cc})[9,10] and by applying the treatment of electric pulses.[11] In this work, we report the coexistence of BRS and URS modes in the Zirconium-doped ZnO thin films. After the forming process, this device with the URS behavior shows either URS mode in the same direction or BRS mode in the opposite direction during the reset process. By controlling different I_{cc} and the span of voltage sweeping in the reset process (V_{stop}), we were able to demonstrate a controllable multilevel storage at LRS and HRS in the ZnO-based device under BRS mode with high density for multi-storage applications.

$Zn_{0.99}Zr_{0.01}O$ thin films were prepared on Pt(111)/Ti/SiO_2/Si substrates using sol-gel method. Zinc acetate and zirconium oxychloride were used as sources, while 2-methoxyethanol and diethanolamine were used as the solvent and the stabilizer, respectively. $Zn_{0.99}Zr_{0.01}O$ thin films were spin-coated and preheated at 350 °C for 10 min. Finally, after the desired thickness (~200 nm) was reached, these thin films were annealed at 550 °C for 30 min in air ambient. For electrical measurements, an array of the top Pt electrode (TE) with a diameter ranging from 200 nm to 200 μm was deposited by magnetron sputtering. The schematic of the Pt/$Zn_{0.99}Zr_{0.01}O$/Pt structure is illustrated in the inset of Fig. 1(a), the bias voltage was applied to TE and the bottom electrode (BE) was grounded. The crystalline orientations of these thin films were characterized by X-ray diffraction (XRD, D/Max 2550, Japan). As shown in Fig. 1(a), the Zr-doped ZnO thin films exhibit a polycrystalline pattern with a highly (002) textured orientation. Electrical measurements were carried using an Agilent B1500A semiconductor parameter analyzer.

In our experiments, the fresh memory cells were always at HRS, with a resistance of ~80 kΩ. A negative voltage was applied to the as-fabricated devices with a I_{cc} of 10 mA to avoid a complete dielectric breakdown. When the applied voltage was ~−2.29 V, soft breakdown occurred, as shown in Fig. 1(b). After the initial forming process, the device with the URS behavior (Fig. 1(c)) can be reversibly switched using either the unipolar operation (Fig. 1(d)) or the bipolar operation method (Fig. 1(e)). When the set process (HRS → LRS) was operated with the voltage of −1.7 V (process 3 in Fig. 1(c)), the reset processes (LRS → HRS) occurred at the voltages of −0.76 V (process 6 in Fig. 1(d)) and +0.71 V (process 4 in Fig. 1(e)). A transition from process 3 to process 6 implies the reproducible URS behavior, while a stable BRS behavior was also observed by applying a positive voltage during the reset process. This suggests that the reproducible RS properties can be achieved in our device with either unipolar or bipolar operation method.

For the unipolar operation method, the URS mode can be explained by the conducting filaments (CF's) formation/rupture controlled by the thermal effects mechanism.[12] Under a negative forming voltage, oxygen ions in the thin film will

[a)]Electronic mail: mhtang@xtu.edu.cn. Tel.: +86-731-58292200. Fax: +86-731-58292468.

 © 2014 AIP Publishing LLC

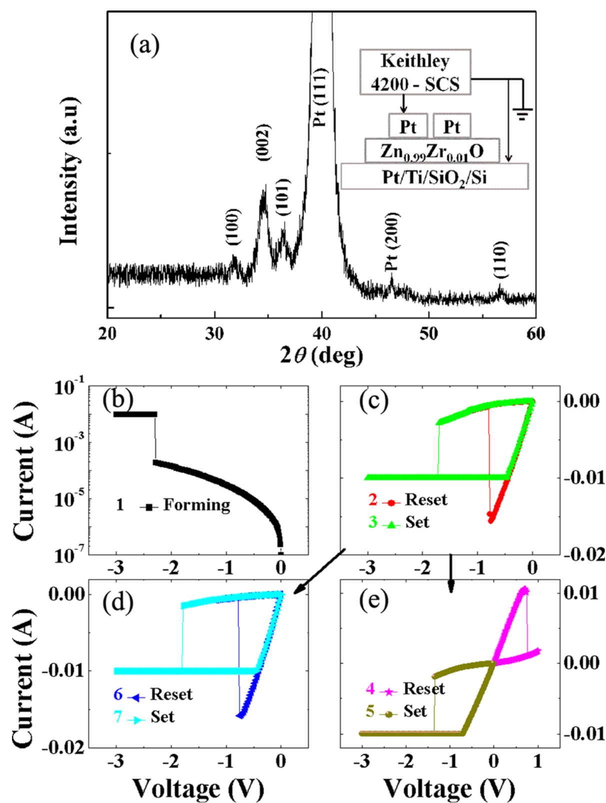

FIG. 1. (a) The typical XRD θ-2θ scan data of Zr-doped ZnO thin films grown on Pt(111)/Ti/SiO_2/Si substrates. The inset shows the schematic structure of the device. (b) The forming process of device with I_{cc} of 10 mA. (c) The URS behavior after forming. (d) The URS mode after using the unipolar operation method. (e) The BRS mode after using the bipolar operation method.

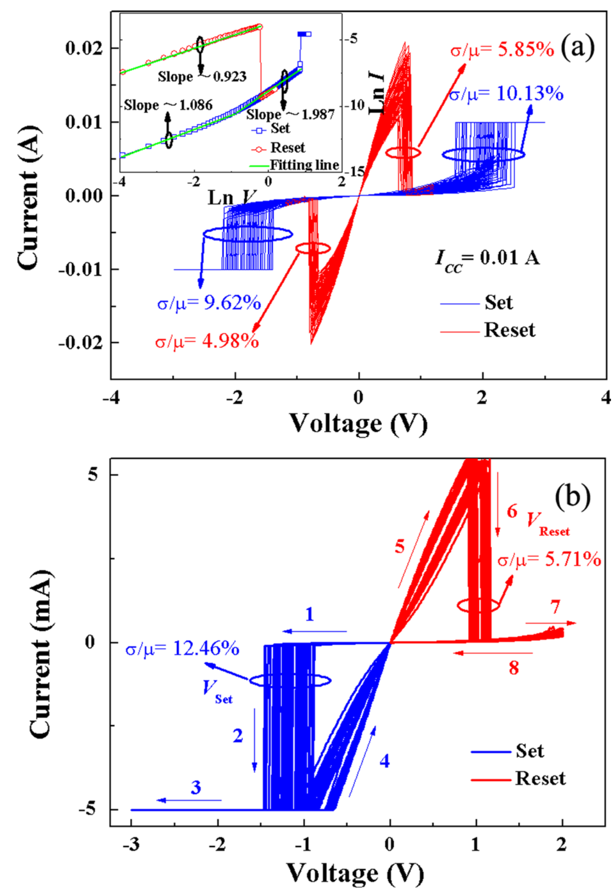

FIG. 2. (a)Typical URS behavior of the Pt/$Zn_{0.99}Zr_{0.01}O$/Pt device with I_{cc} of 10 mA. The inset shows corresponding Ln*I*-Ln*V* curves. (b) The *I*–*V* curves of the BRS behavior of the device with I_{cc} of 5 mA.

move toward the Pt BE. Oxygen vacancies are thus migrated and gathered together to generate CF's, which causes the device switching from HRS to LRS. Subsequently, the CF's are ruptured by local excessive Joule heating due to the occurrence of high current density, the device switches back to HRS. In contrast, for the bipolar operation method, electrochemical migration of oxygen ions under the electrical field is regarded as the driving mechanism.[13] Under positive bias voltages, oxygen ions at the BE could infiltrate back through film to oxidize the oxygen vacancies, giving rise to the rupture of CF's. This causes the device transforming from LRS to HRS. Meanwhile, the thermal-assisted rupture of CF's in the reset process is likely induced by the Joule-heat.[14,15]

It is noted that the forming voltage of the Zr-doped devices is much lower than that (3.8 V) of undoped ZnO devices in our previous report.[7] This could be attributed to the abundant oxygen vacancy clusters pre-existing in thin films, which reduces the value of the forming voltage.[16] Zhang *et al*. reported that there are a lot of oxygen vacancies in the Zr-doped ZnO thin films.[17] Therefore, as reported previously,[18] the doping can be employed to eliminate the forming process and improve the uniformity. As shown in Fig. 2(a), the URS behavior was found stable (216 cycles) and reproducible with R_{HRS}/R_{LRS} ($>10^2$). The distributions of set voltage (V_{Set}) and reset voltage (V_{Reset}) were observed very narrow. Especially, the values of V_{Set} and V_{Reset} for negative voltage region varied from -1.42 V to -2.34 V and from -0.68 V to -0.8 V, respectively. The relative fluctuations (standard deviation (σ)/mean value (μ)) of V_{Set} and V_{Reset} were found to be 9.62%, and 4.98%, respectively. In order to elucidate the mechanism of URS, typical *I*–*V* curves were re-plotted in log-log scale in the inset of Fig. 2(a). In the LRS, the current depends linearly on the voltage with a slope of 0.92, corresponding to the ohmic conduction behavior. However, nonlinear *I*–*V* characteristic appears at higher electric field in HRS. The classical nonlinear conduction mechanisms, including Schottky emission,[19] Poole-Frenkel emission,[20] and space charge limited current (SCLC),[21,22] were all adopted to try to fit the nonlinearity of the measured *I*–*V* relation, and it was found that SCLC has the best fit. At low voltages (<0.32 V), *I*–*V* curve exhibits linear behavior and the conduction behavior is governed by ohmic law. At high voltages (>0.32 V), a rapid current increase is observed with a slope of about 2, which is very similar to the observations reported in Refs. 21 and 22.

By using the bipolar operation method, stable BRS behavior can also be achieved in our devices. We can see from Fig. 2(b) that the BRS mode for a I_{cc} of 5 mA was very uniform in 100 cycles. Bias voltage sweeps were applied under the sweeping sequence of 1 → 8. The values of V_{Set} varied from -0.9 V to -1.47 V with a σ/μ value at 12.46%, while those of V_{Reset} varied from 0.92 V to 1.15 V with a σ/μ value at 5.71%. Meanwhile, the R_{HRS} values were found to be in the range of 18.6–57.3 kΩ with a σ/μ value at 19.75%. However, the fluctuation of R_{LRS} was

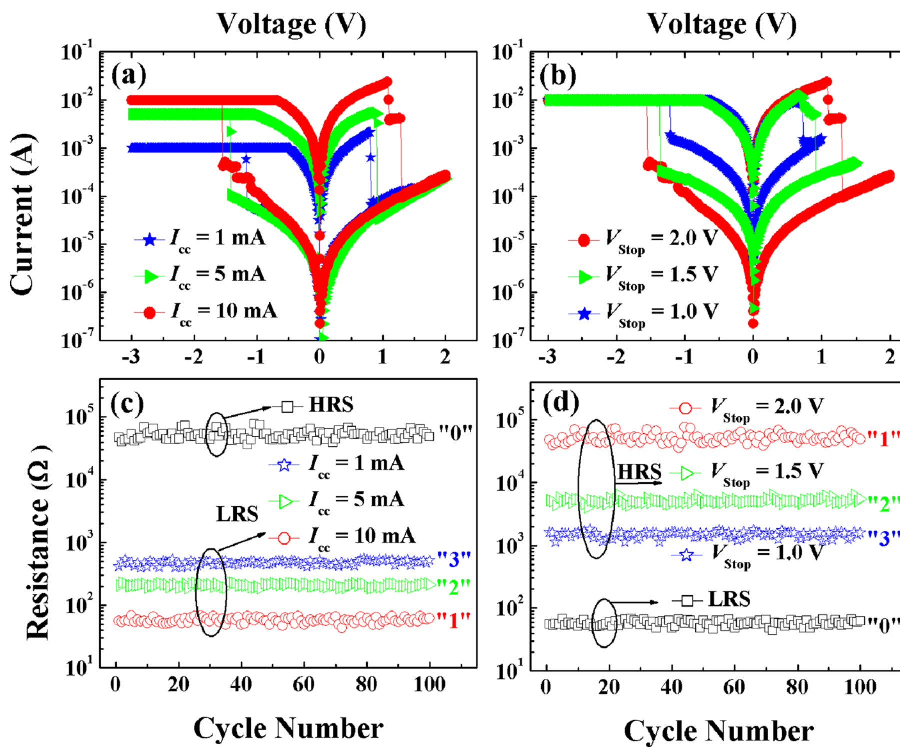

FIG. 3. I–V characteristics of BRS when varying (a) the I_{cc} and (b) the V_{Stop}. Endurance tests of 100 cycles for the BRS when varying (c) the I_{cc} and (d) the V_{Stop}.

found much smaller as compared to that of R_{HRS}, with a σ/μ value of 10.26%.

Furthermore, by varying the values of I_{cc} or V_{stop}, multi-state resistances at LRS or HRS in our devices under the BRS mode can be obtained, respectively. Fig. 3(a) shows the I–V characteristics with different I_{cc} values of 1, 5, and 10 mA, respectively. It was found that varying of I_{cc} could result in different resistances at the LRS. This is because more or stronger CF's are induced by higher I_{cc}. Therefore, the higher I_{cc} was applied, the smaller the resistance at LRS was obtained.[23] As can be observed in Fig. 3(b), the I–V characteristics with different resistances at the HRS could be achieved by varying the V_{stop}. This implies that there are a few residual un-ruptured CF's within the memory film.[23] Therefore, with the further applying of higher positive voltage bias, these residual un-ruptured CF's will be ruptured, causing the device switching to a higher resistance state. It was found that RS was very stable at each memory state with an endurance test of ∼100 cycles for different I_{cc} (Fig. 3(c)) and different V_{stop} (Fig. 3(d)). Fig. 4(a) depicts the I–V curve performed by continuously increasing the bias voltage to various values of V_{stop} (1.0 V, 1.5 V, and 2.0 V). It can be seen that the multilevel HRS can also be obtained in our device. Considering the practical operation for memory applications, the electric-pulse-induced resistance (EPIR) switching test was performed for the device with widths of all pulses set at 200 ns. As indicated in Fig. 4(b), by controlling the amplitude of the erasing voltage pulses, three distinct higher resistance states (2, 3, and 4) were produced, while the bias voltage of switching the device into LRS was fixed at −3 V.

The values of R_{HRS} and R_{LRS} for different device areas can be found in Figs. 5(a) and 5(b). Larger storage windows can be achieved with further scaling down the device area. Again, the multistate resistances at LRS (for different I_{cc}) and HRS (for different V_{stop}) were observed for all devices with different areas. The EPIR change property was further investigated for the device with the cell diameter of 200 nm. Fig. 5(c) shows that all the resistance states of device can be

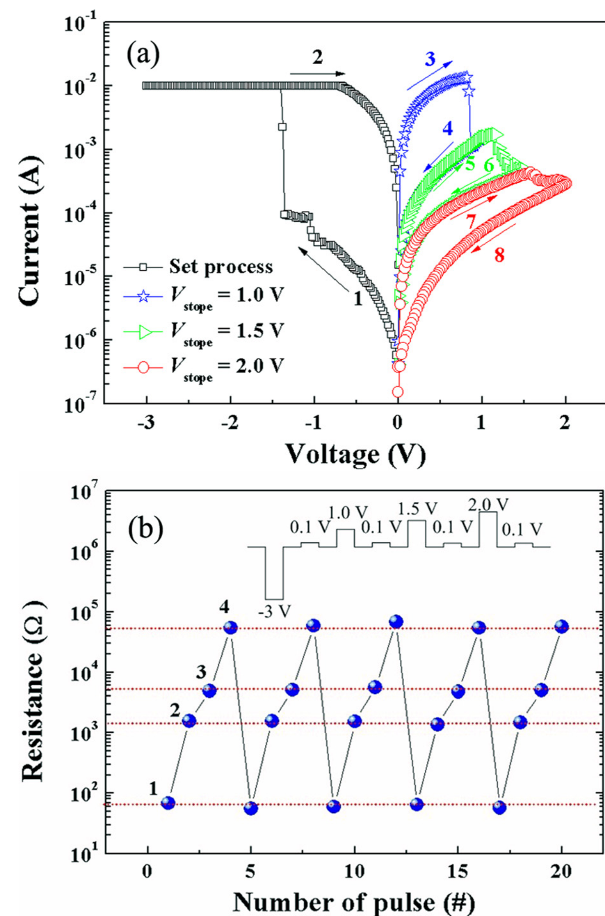

FIG. 4. (a) Multilevel HRS observed by varying V_{Stop} during the reset process. (b) EPIR switching test on the device with cell diameter of 200 μm.

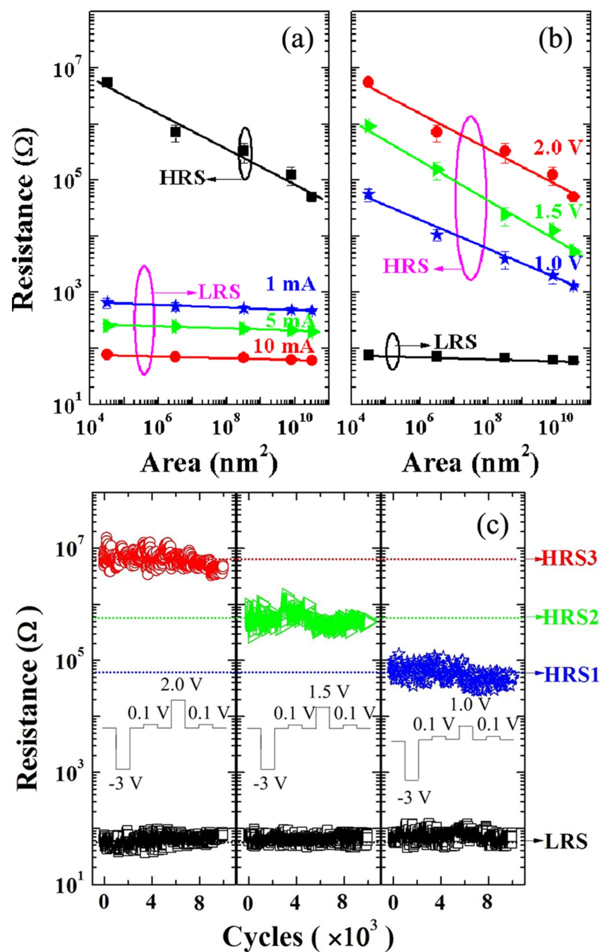

FIG. 5. The resistances of HRS and LRS in the devices with different cell diameter ranging from 200 nm to 200 μm, (a) for different I_{cc} and (b) for different V_{Stop}. (c) Switching cycles in BRS behavior with different erase voltage pulses of the Pt/$Zn_{0.99}Zr_{0.01}O$/Pt device.

repeated over 10^4 cycles with the endurance results measured at 2 V, 1.5 V, and 1 V erasing voltage pulses, respectively. In addition, sufficient sensing margin was also observed in our RRAM device.

This work was financially supported by Project of National Natural Science Foundation of China (NSFC) (Grant No. 61274107) and 973 Program (Grant No. 2012CB326404).

[1]J. J. Yang, D. B. Strukov, and D. R. Stewart, Nat. Nanotechnol. **8**, 13 (2013).
[2]Y. C. Yang, F. Pan, Q. Liu, M. Liu, and F. Zeng, Nano Lett. **9**, 1636 (2009).
[3]Q. Liu, J. Sun, H. B. Lv, S. B. Long, K. B. Yin, N. Wan, Y. T. Li, L. T. Sun, and M. Liu, Adv. Mater. **24**, 1844 (2012).
[4]J. S. Choi, J.-S. Kim, I. R. Hwang, S. H. Hong, S. H. Jeon, S.-O. Kang, B. H. Park, D. C. Kim, M. J. Lee, and S. Seo, Appl. Phys. Lett. **95**, 022109 (2009).
[5]S. C. Chae, J. S. Lee, S. J. Kim, S. B. Lee, S. H. Chang, C. Liu, B. Kahng, H. Shin, D.-W. Kim, H. Shin, C. U. Jung, S. Seo, M.-J. Lee, and T. W. Noh, Adv. Mater. **20**, 1154 (2008).
[6]X. W. Sun, G. Q. Li, X. A. Zhang, L. H. Ding, and W. F. Zhang, J. Phys. D: Appl. Phys. **44**, 125404 (2011).
[7]M. H. Tang, B. Jiang, Y. G. Xiao, Z. Q. Zeng, Z. P. Wang, J. C. Li, and J. He, Microelectron. Eng. **93**, 35 (2012).
[8]H. Y. Peng, G. P. Li, J. Y. Ye, Z. P. Wei, Z. Zhang, D. D. Wang, G. Z. Xing, and T. Wu, Appl. Phys. Lett. **96**, 192113 (2010).
[9]Y. T. Lee, H. Kim, J. Park, and K. Yong, J. Appl. Phys. **108**, 076101 (2010).
[10]D. L. Xu, Y. Xiong, M. H. Tang, and B. W. Zeng, J. Alloys Compd. **584**, 269 (2014).
[11]L. L. Wei, J. Wang, Y. S. Chen, D. S. Shang, Z. G. Sun, B. G. Shen, and J. R. Sun, J. Phys. D: Appl. Phys. **45**, 425303 (2012).
[12]S. H. Chang, S. C. Chae, S. B. Lee, C. Liu, T. W. Noh, J. S. Lee, B. Kahng, J. H. Jang, M. Y. Kim, D. W. Kim, and C. U. Jung, Appl. Phys. Lett. **92**, 183507 (2008).
[13]K. Szot, W. Speier, G. Bihlmayer, and R. Waser, Nature Mater. **5**, 312 (2006).
[14]Y. C. Yang, F. Pan, and F. Zeng, New J. Phys. **12**, 023008 (2010).
[15]X. J. Zhu, C. S. Ong, X. X. Xu, B. L. Hu, J. Shang, H. L. Yang, S. Katlakunta, Y. W. Liu, X. X. Chen, L. Pan, J. Ding, and R.-W. Li, Sci. Rep. **3**, 1084 (2013).
[16]N. Xu, L. F. Liu, X. Sun, X. Y. Liu, D. D. Han, Y. Wang, R. Han, J. F. Kang, and B. Yu, Appl. Phys. Lett. **92**, 232112 (2008).
[17]J. Zhang, D. Q. Gao, G. J. Yang, J. L. Zhang, Z. H. Shi, Z. H. Zhang, Z. H. Zhu, and D. S. Xue, Nanoscale Res. Lett. **6**, 587 (2011).
[18]Q. Liu, S. B. Long, W. Wang, Q. Y. Zuo, S. Zhang, J. N. Chen, and M. Liu, IEEE Electron Device Lett. **30**, 1335 (2009).
[19]Y. T. Chen, T. C. Chang, P. Jiang, J. J. Huang, H. C. Tseng, P. C. Yang, A. K. Chu, J. B. Yang, H. C. Huang, D. S. Gan, M. J. Tsai, and S. M. Sze, Appl. Phys. Lett. **102**, 043508 (2013).
[20]C. C. Lin, Z. L. Tseng, K. Y. Lo, C. Y. Huang, C. S. Hong, S. Y. Chu, C. C. Chang, and C. J. Wu, Appl. Phys. Lett. **101**, 203501 (2012).
[21]J. Zhang, H. Yang, Q. L. Zhang, S. R. Dong, and J. K. Luo, Appl. Phys. Lett. **102**, 012113 (2013).
[22]X. M. Chen, G. H. Wu, P. Jiang, W. F. Liu, and D. H. Bao, Appl. Phys. Lett. **94**, 033501 (2009).
[23]S. Y. Wang, C. W. Huang, D. Y. Lee, T. Y. Tseng, and T. C. Chang, J. Appl. Phys. **108**, 114110 (2010).

Applied Physics Letters is copyrighted by the American Institute of Physics (AIP).
Redistribution of journal material is subject to the AIP online journal license and/or AIP copyright. For more information, see http://ojps.aip.org/aplo/aplcr.jsp